

This is the accepted manuscript made available via CHORUS. The article has been published as:

Origin of the anomalous Pb-Br bond dynamics in formamidinium lead bromide perovskites

Harishchandra Singh, Ruixiang Fei, Yevgeny Rakita, Michael Kulbak, David Cahen, Andrew M. Rappe, and Anatoly I. Frenkel

Phys. Rev. B **101**, 054302 — Published 10 February 2020

DOI: [10.1103/PhysRevB.101.054302](https://doi.org/10.1103/PhysRevB.101.054302)

Origin of the anomalous Pb-Br bond dynamics in FAPbBr₃ perovskites

Harishchandra Singh,¹ Ruixiang Fei,² Yevgeny Rakita,³ Michael Kulbak,³ David Cahen,³

Andrew M. Rappe,^{2,*} Anatoly I. Frenkel^{1,&}

¹*Department of Materials Science and Chemical Engineering, Stony Brook University, Stony Brook, NY 11794, USA*

²*Department of Chemistry, University of Pennsylvania, Philadelphia, PA 19104-6323, USA*

³*Department of Materials and Interfaces, Weizmann Institute of Science, Rehovot 76100 Israel*

Abstract

Extended X-ray absorption fine structure spectroscopy of the light-harvesting formamidinium lead bromide (FAPbBr₃) perovskite, a system with attractive optoelectronic performance, shows anomalously large variance in Pb-Br bond length, some 50% larger than in its inorganic CsPbBr₃ counterpart. Using first-principles molecular dynamics simulations, we find a significant contribution to this variance coming from the FA cation, and show that the FA does not just tumble in its cuboctahedral Br₁₂ cage, but instead stochastically sticks to, and detaches from one of the twelve nearest Br atoms after another, leading to the large variance in Pb-Br bond length. Our results demonstrate dynamic coupling between the FA-Br moiety and perovskite cage vibrations, and that tunability in dynamics can be achieved by changing the cation type and perovskite lattice parameter. Thus, our results provide new information that needs to be considered in any of the intensely debated models of electron-phonon coupling in lead halide perovskites.

I. INTRODUCTION

Owing to their unique electronic properties and contribution to outstanding power conversion efficiencies of solar cells, organic and inorganic lead-halide perovskites (e.g. FAPbX_3 , MAPbX_3 and CsPbX_3 , where formamidinium (FA) and methylammonium (MA) are the organic components and X is a halogen, Cl/Br/I) are the focus of intense theoretical and experimental investigations [1-6]. The sources of the observed structural disorder [7-15], and their possible correlations with optoelectronic properties in these perovskites are intensely debated [8,13,16,17]. Because it has been shown that those properties are defined by the metal-halogen interactions [13,18], understanding the detailed behavior of the Pb- X bond length disorder may well help to provide a solid basis for the relation between mechanical and optoelectronic properties of these materials. The samples selected for this study are the well-characterized organic lead-halide FAPbBr_3 and inorganic lead-halide CsPbBr_3 materials, both of which contain Pb-Br bonds. By combining extended X-ray absorption fine structure (EXAFS) spectroscopy with *ab initio* molecular dynamics simulations (MD), we align model-independent measurements of the disorder in these perovskites with atomic- and electronic-scale interpretation and analysis, highlighting the influence of the organic cations on the dynamics of the inorganic framework.

The samples were thin films, CsPbBr_3 (50 nm) and FAPbBr_3 (500 nm), spin-coated onto a glass microslide; details on fabrication can be found in Supplementary Material [19] (see, also, references [20-30] therein). EXAFS measurements at Pb L_3 - and Br K- edges allowed us to focus on these atomic species (Pb and Br). Pb and Br form bonds along all the edges of the perovskite unit cell (Fig. 1) forming the structural framework common to the organic and inorganic perovskites. Therefore, probing these Pb-Br bonds by comparing their vibrational properties in these two systems gives a sensitive probe of structural dynamics.

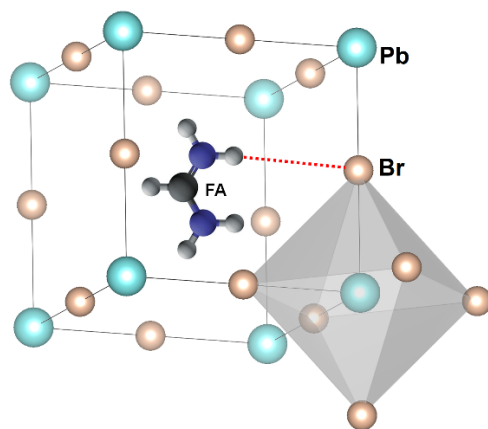


FIG. 1. Schematic of the FAPbBr₃ structure. Dashed line denotes the *shortest* instantaneous H-Br distance during the rotation of an FA cation.

EXAFS measurements at the Pb L₃-edge (13.035 keV) and Br K-edge (13.474 keV) were collected at the 5BM DND CAT beamline at the Advanced Photon Source (APS) of the Argonne National Laboratory, where a four-channel Vortex detector has been used to collect the fluorescence data. EXAFS data were processed using conventional procedures, as described in Supplementary Material.

II. RESULTS AND DISCUSSION

The k^2 -weighted EXAFS data for Pb and Br edges for both samples are shown in k -space [see Supplemental Material, Fig. S1] and r -space (Fig. 2). The Br K edge spectra have a split first shell peak in r -space (Fig. 2 b), due to the Ramsauer-Townsend effect in the backscattering amplitude of Pb [31]. The main effect, evident in the k -space and r -space data of both Br and Pb edges, is the strong decrease of the signal intensity of the FAPbBr₃ sample compared to that in the CsPbBr₃ sample. We briefly outline possible causes for these changes that we will quantitatively analyze in the subsequent section. One reason for this effect could be the decrease in the Pb-Br (and Br-Pb) coordination number in the organic sample, compared to the inorganic one. Another reason for this effect could be the relative increase of the Pb-Br bond length disorder in the organic sample. However, the change in the coordination numbers is not reasonable in three-dimensional perovskites, as the Pb environment remains hexadentate. An enhanced disorder in the organic sample is, thus, the most reasonable explanation for the data. We have also examined, and subsequently ruled out, the X-ray beam damage effect as a possible cause of the changes in the

organic sample EXAFS spectra compared to the inorganic ones (see Supplementary Material, Figs. S2 and S3).

Because EXAFS measurement provides almost instantaneous “snapshots” of the structure (with characteristic time of each snapshot of ≈ 1 fs), information about bond dynamics is stored in the EXAFS spectra via the mean-squared disorder σ_{dyn}^2 . If static (configurational) disorder σ_{st}^2 is present as well as dynamic disorder, and it is statistically independent of σ_{dyn}^2 , then both types of disorder will contribute to the total disorder: $\sigma^2 = \sigma_{\text{st}}^2 + \sigma_{\text{dyn}}^2$, which is measured by EXAFS. To understand the nature of the dramatic intensity change (Fig. 2) observed in these materials, we focused on the investigation of the dynamic behavior, by combining quantitative EXAFS analysis and MD simulations.

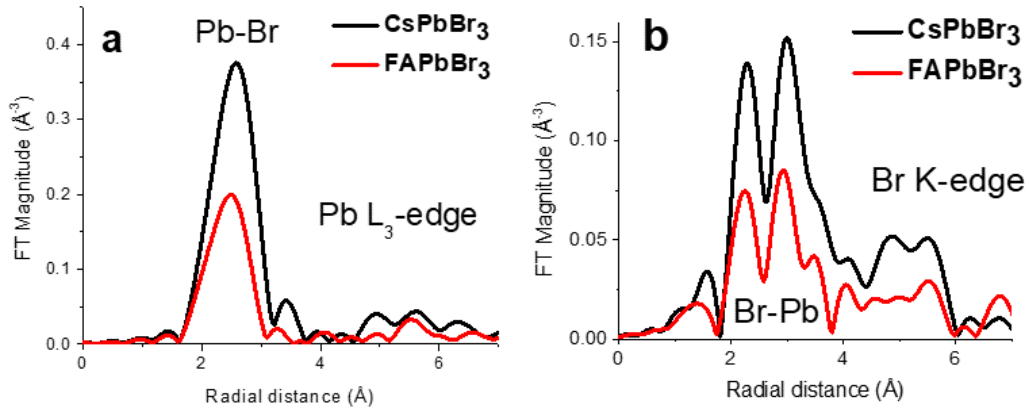


FIG. 2. Fourier transform magnitudes of the Pb L_3 edge (a) and Br K edge (b) k^2 -weighted EXAFS data for CsPbBr_3 and FAPbBr_3 samples.

The resultant EXAFS signals were analyzed in r -space using FEFF6 [32] and Artemis codes from the Demeter package [33]. For the Br edge, the Br-Pb first nearest-neighbor path, and for the Pb edge – the Pb-Br paths were included in their respective fits. The details of the FEFF calculations, fitting model and Fourier transform parameters used in the fits are summarized in the Supplementary material. The data and fits to the Pb L_3 and Br K edge spectra in both samples are shown in Supplemental Material, Fig. S4 in r -space. Consistent with the visual observation (Fig. 2), the values of the Pb-Br bond length disorder in the organic perovskite sample were obtained to be approximately 50% larger than in the inorganic one: $\sigma_{\text{FA}}^2 = 0.0209 \pm 0.0013 \text{ \AA}^2$ vs. $\sigma_{\text{CS}}^2 = 0.0144 \pm 0.0019 \text{ \AA}^2$.

This difference between the disorder parameters ($0.0065 \pm 0.0023 \text{ \AA}^2$) of the Pb-Br bond is comparable to that ($0.0041 \pm 0.0007 \text{ \AA}^2$) reported for another bond type, Rb-Cl, which is a common bond in two types of alkali halides, RbCl and Rb(Br,Cl), a solid solution of RbBr and RbCl, that were measured by EXAFS at 30 K [34]. In those materials, the larger σ^2 value of $0.0096 \pm 0.0005 \text{ \AA}^2$ was found in the mixed system and its difference from the corresponding value ($0.0055 \pm 0.0005 \text{ \AA}^2$) in pure RbCl was attributed to bond buckling [34], due to loss of contact of the smaller Cl⁻ (compared to Br⁻) anions with their Rb neighbors in the octahedral cage. In the present case, the measurement of the Pb-Br disorder parameter is not sufficient to describe the complicated structural dynamics of FAPbBr₃ (or CsPbBr₃) and discriminate between possible models of disorder that may include rotation or, as it was recently shown, the tumbling motion of FA cation in FAPbX₃ cage [35]. To address this challenge, we performed first-principles MD simulations based on density functional theory (DFT) [24-29]. These calculations were performed at 300 K, using lattice parameters of the orthorhombic and cubic CsPbBr₃ unit cells and cubic FAPbBr₃ unit cell (see Supplementary Material). To obtain the velocity autocorrelations, the time intervals were 40 ps long, with a 10 fs time step for inorganic perovskites, and 25 ps long, with 2 fs time step for organic perovskites. We verified that, at this simulation length, the velocity autocorrelation converged.

We now focus on the two possible factors that differ between the two investigated systems: a) the cation type (Cs vs FA) and b) the lattice parameter. The Cs-FA substitution, accompanied by the phase change from orthorhombic CsPbBr₃ to cubic FAPbBr₃, coupled with the difference in the effective cation size (causing greater lattice parameter in FAPbBr₃) could have a complex effect on the bond length disorder. To model the lattice expansion effect, we systematically calculated the changes in the p-DOS for different amounts of deformation (see also Supplementary material, Table S1), denoted as strain 1 and strain 2. The strain 1 represents the CsPbBr₃, strained from an orthorhombic ($a=11.659$, $b=11.735$, $c=11.594 \text{ \AA}$) to a cubic phase ($a=11.735 \text{ \AA}$). We find that the phonon frequencies decrease with increasing tensile strain (Fig. 3a), and that the Pb-Br bond length disorder increases with strain (Fig. 3b). Once the p-DOS $\rho_R(\omega)$, the vibrational density of states, projected on the bond direction R , is obtained, the mean-square relative displacement (MSRD), also known as the EXAFS Debye–Waller factor, σ_R^2 ,

is given by the Debye integral $\sigma_R^2 = \frac{\hbar}{2\mu_R} \int_0^{\omega_{max}} d\omega \rho_R(\omega) \frac{\coth \frac{\beta \hbar \omega}{2}}{\omega}$, where μ_R is the reduced mass

of Pb-Br pair, $\frac{1}{\mu_R} = \frac{1}{M_{Pb}} + \frac{1}{M_{Br}}$, and $\beta = 1/k_B T$ [36]. As calculated over the p-DOS, the values of the Pb-Br bond length disorder were obtained to be $\sigma_{Cs}^2 = 0.0133 \pm 0.0004 \text{ \AA}^2$ for orthorhombic CsPbBr₃ and $0.0182 \pm 0.0006 \text{ \AA}^2$ for cubic CsPbBr₃, using the lattice constant of FAPbBr₃ at room temperature. However, the simulated disorder value for the FAPbBr₃ was found to be $\sigma_{FA}^2 = 0.0210 \pm 0.0006 \text{ \AA}^2$ (Fig. 3b) which is significantly larger than that of cubic CsPbBr₃ (with the same axes ratios and lengths). In addition, the simulated and the experimental disorder values ($0.0209 \pm 0.0013 \text{ \AA}^2$ for the cubic FAPbBr₃ and $0.0144 \pm 0.0019 \text{ \AA}^2$ for the orthorhombic CsPbBr₃) are in remarkable agreement. Hence, one can be confident that the enhanced disorder of cubic FAPbBr₃ must have a significant and direct contribution from the organic moiety (Fig. 3b), namely the FA makes a large contribution to the Pb-Br bond disorder in the cubic phase.

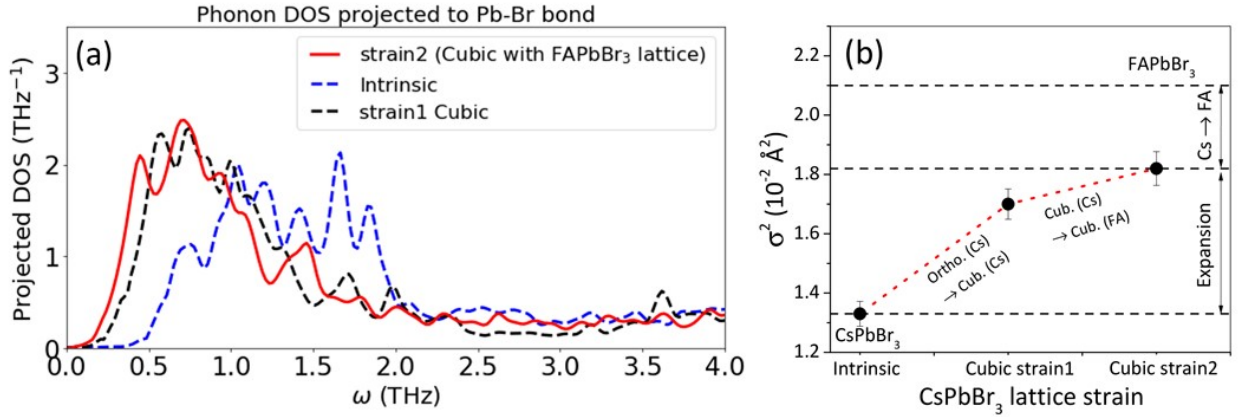


FIG. 3 The phonon density of state (DOS) of CsPbBr₃ projected to the Pb-Br bonds (a), and the mean square relative displacements (σ^2) of Pb-Br distances in CsPbBr₃ at room temperature for different lattice constants and symmetries, calculated using MD simulations (b). Simulated σ^2 value for FAPbBr₃ is shown as well. This computational exploration of inorganic perovskite CsPbBr₃ illustrates two key aspects contributing to enhanced bond disorder in the hybrid perovskite FAPbBr₃, the expansion of the lattice and the compositional substitution.

MD simulations provide insight into the origin of this enhanced dynamic disorder in the hybrid perovskite. Figure S5a illustrates the conventional bond length dynamics in cubic CsPbBr₃, in which the Pb-Br and Br-Cs pairs oscillate about their average lengths calculated from the MD trajectory using eight formula unit supercells. The variation range of Pb-Br bond length is 0.3 \AA in CsPbBr₃ (Fig. S5a), in striking contrast with the Pb-Br bond length behavior in FAPbBr₃ (Fig.

S3b) that exhibits much larger fluctuations. Figure 4a reveals that large variations of the Pb-Br bond lengths correlate with the strongly non-rotational “sticky” motion of FA cation. This conclusion is deduced from the negative value (at $\Delta t = 0$) of the normalized cross-correlation function of the Pb-Br and H-Br shortest distances containing the same Br atom. Figure S5b plots the time-dependence of the H-Br distances, which connect a given Br atom with the nearest H atom in a given FA cation. *This strong anticorrelation means that a particularly short H-Br bond frequently occurs at the same time when the Br-Pb bond is elongated, suggesting that the interactions of the organic cation with Br influence the Pb-Br structure backbone.* In Fig. 4b, we compare the shortest H-Br distance calculated from the MD trajectory over the entire simulation box with that from the simple hypothetical rotational motion of FA cation. This demonstrates that this cation displaces off-center and H-bonds are formed, leading to shorter H-Br bonds than expected. The details of these calculations are given in Supplementary Material.

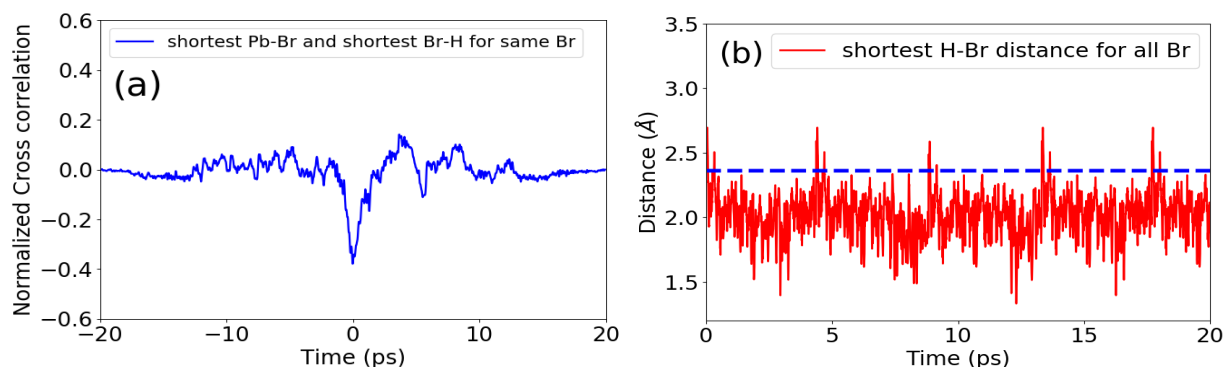


FIG. 4. (a) The normalized cross-correlation function of the shortest H-Br distances and the Pb-Br distances for the same Br atom in FAPbBr_3 , calculated from the MD trajectory. The negative value at $\Delta t = 0$ indicates that the formation of the shortest Br-H bonds coincides in time with elongation of the Pb-Br bonds for the same Br atoms. (b) The shortest H-Br for the Pb_8 nearest-neighbor cube, calculated from the MD trajectory of FAPbBr_3 . The dashed line is the shortest H-Br distance calculated using a hypothetical rigid rotational motion of the FA ion around the FA center of mass that stays at the cage center.

We obtained larger changes for the shorter Pb-Br distance of the two bonds between any Br atom and its nearest Pb neighbors and, hence, Fig. S3b, shows only the shortest Pb-Br distance behavior. As shown in Fig. 4b, FA spends significant time (on average, 91%) by sticking and remaining close to one of the 12 nearest Br atoms. In this respect, the FA cation is almost never

located in the FABr_{12} cuboctahedron center, corresponding to the average structure. Instead, it is locally displaced from the center of FA mass, stochastically sticking to, and separating from one of the nearest 12 Br atoms. This model has some fascinating similarities with the order-disorder “eight site model” [37,38], in which the central Ti atoms in the high-temperature phase of BaTiO_3 are located at the TiO_6 octahedron centers only on average, while locally all Ti atoms are displaced in one of the eight (111) lattice directions.

Whereas discrete rotational reorientations of FA cation in FAPbI_3 perovskite were detected by MD simulations before [39], our MD simulations, combined with our experimental EXAFS results, evidence for the first time the direct impact of the anomalous FA-X dynamics on the cage vibration. Results of our combined analysis fully explain the observed increase of the Pb-Br bond length disorder in the FAPbBr_3 compared to CsPbBr_3 . The good quantitative agreement between theory and experiment for the MSD values of both orthorhombic CsPbBr_3 and cubic FAPbBr_3 allowed us to rely on the details of MD simulations to disentangle between the different possible contributions to lattice dynamics of the Pb-Br cage. Our results demonstrate that the Pb-Br disorder in both compounds is predominantly dynamic, in good agreement with both the hypothesis made above on the basis of the difference in the structures and on the conclusion, drawn from the temperature dependence of the Urbach energy of MAPbI_3 , i.e., that it results dominantly from dynamic disorder (originating from the cage vibration), rather than from static disorder [40]. As a result, we are able to evaluate quantitatively the effects on the bond length disorder due to the lattice parameter change between the different structures and to evaluate the specific contribution for the cation at the *A* site (Cs – FA substitution) on the bond dynamics. Our MD simulations show that the composition-specific effect of FA on the Pb-Br bond dynamics is responsible for ~50% of the enhancement of the total disorder, whereas the remaining half is attributed to the contribution to dynamics due to the lattice expansion. A close look at the details of MD simulations reveals that FA spends most of the time sticking close to a Br atom via hydrogen bonding, causing significant perturbations in Pb-Br bond lengths during those time intervals. These results emphasize the significance of the perturbations coming from FA-X interactions for explaining the enhanced dynamic disorder of Pb-Br in FAPbBr_3 compared to CsPbBr_3 .

III. SUMMARY

Our results, which demonstrate dynamic coupling between the Pb-*X* and FA-*X* moieties, provide new information on possible energy transfer mechanisms and the related intensely debated models of electron-lattice coupling in lead halide perovskites [41,42]. One such model links large carrier lifetime in MAPbI₃ to dynamic motion (*rotation*) of MA molecule at the picosecond time scale [43]. Stochastic, picosecond-long, *sticking* motion of the FA molecule can be similarly important for explaining the carrier lifetime in the FAPbBr₃, one of the unresolved challenges [44]. In addition, our findings pose challenge to the polaron concept, a commonly used recent model, to explain mobility in halide perovskites [44]. Characteristic time constants for polaron formation for organic and inorganic halide perovskites range between 0.3 and 0.7 ps [45], i.e., the same time scale as the sticking time we observed in FAPbBr₃ system. The FA “stickiness”, which is affected strongly by the volume of the lattice, will also contribute to the anharmonicity in Pb-*X* vibrations, and thus directly affect charge mobility, thermal conductivity [46] and mechanical stability of FAPbX₃ perovskites [47].

ACKNOWLEDGEMENTS

AIF acknowledges support by National Science Foundation Grant number DMR-1911592. RF and AMR acknowledge support from the National Science Foundation, under grant DMR-1719353. Computational support was provided by the National Energy Research Scientific Computing Center of the Department of Energy. X-ray absorption spectroscopy data were collected at the DuPont-Northwestern-Dow Collaborative Access Team (DND-CAT) located at Sector 5 of the Advanced Photon Source (APS). DND-CAT is supported by Northwestern University, E.I. DuPont de Nemours & Co., and The Dow Chemical Company. This research used resources of the Advanced Photon Source, a U.S. Department of Energy (DOE) Office of Science User Facility operated for the DOE Office of Science by Argonne National Laboratory under Contract No. DE-AC02-06CH11357. AIF and AMR acknowledge support by Weston Visiting Professorships during their stays at the Weizmann Institute of Science. YR and DC thank the US-Israel Binational Science Foundation, the Ullmann family foundation and the Weizmann Institute’s Sustainability and Energy Research Initiative for partial support.

Corresponding authors:

* rappe@sas.upenn.edu

& anatoly.frenkel@stonybrook.edu

References

- [1] D. B. Mitzi, *Chem. Rev.* **119**, 3033 (2019).
- [2] A. K. Jena, A. Kulkarni, and T. Miyasaka, *Chem. Rev.* **119**, 3036 (2019).
- [3] Q. Tai, K.-C. Tang, and F. Yan, *Energy Environ. Sci.* **12**, 2375 (2019).
- [4] H. Tsai, R. Azadpour, J.-C. Blancon, C. C. Stoumpos, O. Durand, J. W. Strzalka, B. Chen, R. Verduzco, P. M. Ajayan, S. Tretiak, *et al.*, *Science* **360**, 67 (2018).
- [5] Q. A. Akkerman, G. Rainò, M. V. Kovalenko, and L. Manna, *Nature Mater.* **17**, 394 (2018).
- [6] J. Huang, Y. Yuan, Y. Shao, and Y. Yan, *Nature Rev. Mater.* **2**, 17042 (2017).
- [7] S. Kanno, Y. Imamura, and M. Hada, *J. Phys. Chem. C* **121**, 26188 (2017).
- [8] M. Fu, P. Tamarat, J.-B. Trebbia, M. I. Bodnarchuk, M. V. Kovalenko, J. Even, and B. Lounis, *Nature Commun.* **9**, 3318 (2018).
- [9] A. Poglitsch and D. Weber, *J. Phys. Chem. Lett.* **87**, 6373 (1987).
- [10] A. M. A. Leguy, A. R. Goñi, J. M. Frost, J. Skelton, F. Brivio, X. Rodriguez-Martinez, O. J. Weber, A. Pallipurath, M. I. Alonso, M. Campoy-Quiles, *et al.*, *Phys. Chem. Chem. Phys.* **18**, 27051 (2016).
- [11] O. Selig, A. Sadhanala, C. Muller, R. Lovrincic, Z. Chen, Y. L. A. Rezus, J. M. Frost, T. L. C. Jansen, and A. A. Bakulin, *J. Am. Chem. Soc.* **139**, 4068 (2017).
- [12] Y. S. Guo, O. Yaffe, D. W. Paley, A. N. Beecher, T. D. Hull, G. Szpak, J. S. Owen, L. E. Brus, and M. A. Pimenta, *Phys. Rev. Mater.* **1**, 042401 (R) (2017).
- [13] O. Yaffe, Y. Guo, L. Z. Tan, D. A. Egger, T. Hull, C. C. Stoumpos, F. Zheng, T. F. Heinz, L. Kronik, M. G. Kanatzidis, *et al.*, *Phys. Rev. Lett.* **118**, 136001 (2017).
- [14] M. Z. Mayers, L. Z. Tan, D. A. Egger, A. M. Rappe, and D. R. Reichman, *Nano Lett.* **18**, 8041 (2018).
- [15] X. Wu, L. Z. Tan, X. Shen, T. Hu, K. Miyata, M. T. Trinh, R. Li, R. Coffee, S. Liu, D. A. Egger, *et al.*, *Sci. Adv.* **3**, e1602388 (2017).
- [16] F. Panzer, C. Li, T. Meier, A. Kohler, and S. Huettnner, *Adv. Energy Mater.* **7**, 1700286 (2017).
- [17] S. Singh, C. Li, F. Panzer, K. L. Narasimhan, A. Graeser, T. P. Gujar, A. Kohler, M. Thelakkat, S. Huettnner, and D. Kabra, *J. Phys. Chem. Lett.* **7**, 3014 (2016).
- [18] Z. Xiao and Y. Yan, *Adv. Energy Mater.* **7**, 1701136 (2017).
- [19] See Supplemental Material at <http://> for technical details on sample preparation, EXAFS data, processing and analysis results, and details on DFT and MD calculations.
- [20] Y. Rakita, N. Kedem, S. Gupta, A. Sadhanala, V. Kalchenko, M. L. Bohm, M. Kulbak, R. H. Friend, D. Cahen, and G. Hodes, *Crystal Growth Des.* **16**, 5717 (2016).
- [21] M. Kulbak, S. Gupta, N. Kedem, I. Levine, T. Bendikov, G. Hodes, and D. Cahen, *J. Phys. Chem. Lett.* **7**, 167 (2016).
- [22] M. Kulbak, D. Cahen, and G. Hodes, *J. Phys. Chem. Lett.* **6**, 2452 (2015).
- [23] M. Newville, P. Livins, Y. Yacoby, J. J. Rehr, and E. A. Stern, *Phys. Rev. B* **47**, 14126 (1993).
- [24] P. Giannozzi, S. Baroni, N. Bonini, M. Calandra, R. Car, C. Cavazzoni, D. Ceresoli, G. L. Chiarotti, M. Cococcioni, I. Dabo, *et al.*, *J. Phys.: Condens. Matt.* **21**, 395502 (2009).
- [25] J. P. Perdew, K. Burke, and M. Ernzerhof, *Phys. Rev. Lett.* **77**, 3865 (1996).
- [26] N. J. Ramer and A. M. Rappe, *Phys. Rev. B* **59**, 12471 (1999).
- [27] A. M. Rappe, K. M. Rabe, E. Kaxiras, and J. D. Joannopoulos, *Phys. Rev. B* **41**, 1227 (1990).
- [28] W. G. Hoover, *Phys. Rev. A* **31**, 1695 (1985).
- [29] S. Nosé, *J. Chem. Phys.* **81**, 511 (1984).
- [30] F. C. Hanusch, E. Wisenmayer, E. Mankel, A. Binek, P. Angloher, C. Fraunhofer, N. Giesbrecht, J. M. Feckl, W. Jaegermann, D. Johrendt, *et al.*, *J. Phys. Chem. Lett.* **5**, 2791 (2014).
- [31] A. G. McKale, B. W. Veal, A. P. Paulikas, and S. K. Chan, *Phys. Rev. B* **38**, 10919 (1988).
- [32] S. I. Zabinsky, J. J. Rehr, A. Ankudinov, R. C. Albers, and M. J. Eller, *Phys. Rev. B* **52**, 2995 (1995).
- [33] B. Ravel and M. Newville, *J. Synchrotron Radiat.* **12**, 537 (2005).
- [34] A. Frenkel, E. A. Stern, A. Voronel, M. Qian, and M. Newville, *Phys. Rev. Lett.* **71**, 3485 (1993).

- [35] D. Ghosh, P. Walsh Atkins, M. S. Islam, A. B. Walker, and C. Eames, *ACS Energy Lett.* **2**, 2424 (2017).
- [36] F. D. Vila, J. J. Rehr, H. H. Rossner, and H. J. Krappe, *Phys Rev B* **76**, 014301 (2007).
- [37] I. B. Bersuker, *Phys. Lett.* **20**, 589 (1966).
- [38] R. Comes, M. Lambert, and A. Guinier, *Solid State Commun.* **6**, 715 (1968).
- [39] V. C. A. Taylor, D. Tiwari, M. Duchi, P. M. Donaldson, I. P. Clark, D. J. Fermin, and T. A. A. Oliver, *J. Phys. Chem. Lett.* **9**, 895 (2018).
- [40] M. Ledinsky, T. Schönfeldová, J. Holovský, E. Aydin, Z. Hájková, L. Landová, N. Neyková, A. Fejfar, and S. De Wolf, *J. Phys. Chem. Lett.* **10**, 1368 (2019).
- [41] P.-A. Mante, C. C. Stoumpos, M. G. Kanatzidis, and A. Yartsev, *Nature Commun.* **8**, 14398 (2017).
- [42] A. D. Wright, C. Verdi, R. L. Milot, G. E. Eperon, M. A. Pérez-Osorio, H. J. Snaith, F. Giustino, M. B. Johnston, and L. M. Herz, *Nature Commun.* **7**, 11755 (2016).
- [43] J. Gong, M. Yang, X. Ma, R. D. Schaller, G. Liu, L. Kong, Y. Yang, M. C. Beard, M. Lesslie, Y. Dai, *et al.*, *J. Phys. Chem. Lett.* **7**, 2879 (2016).
- [44] X.-Y. Zhu and V. Podzorov, *J. Phys. Chem. Lett.* **6**, 4758 (2015).
- [45] K. Miyata, T. L. Atallah, and X.-Y. Zhu, *Sci. Adv.* **3**, e1701469 (2017).
- [46] X. Qian, X. Gu, and R. Yang, *App. Phys. Lett.* **108**, 063902 (2016).
- [47] S. Sun, F. H. Isikgor, Z. Deng, F. Wei, G. Kieslich, P. D. Bristowe, J. Ouyang, and A. K. Cheetham, *ChemSusChem* **10**, 3740 (2017).